Optical MIMO-OFDM With Generalized LED Index Modulation

Anil Yesilkaya, *Student Member, IEEE*, Ertugrul Basar, *Senior Member, IEEE*,
Farshad Miramirkhani, *Member, IEEE*, Erdal Panayirci, *Life Fellow, IEEE*,
Murat Uysal, *Senior Member, IEEE*, and Harald Haas, *Senior Member, IEEE*

Abstract—Visible light communications (VLC) is a promising and uncharted new technology for the next generation of wireless communication systems. This paper proposes a novel generalized light emitting diode (LED) index modulation method for multiple-input-multiple-output (MIMO) orthogonal frequency division multiplexing (OFDM)-based VLC systems. The proposed scheme avoids the typical spectrum efficiency losses incurred by time- and frequency-domain shaping in OFDM signals. This is achieved by exploiting spatial multiplexing along with LED index modulation. Accordingly, real and imaginary components of the complex time-domain OFDM signals are separated first, then resulting bipolar signals are transmitted over a VLC channel by encoding sign information in LED indexes. As a benchmark, we demonstrate the performance analysis of our proposed system for both analytical and physical channel models. Furthermore, two novel receiver designs are proposed. Each one is suitable for frequency-flat or selective channel scenarios. It has been shown via extensive computer simulations that the proposed scheme achieves considerably better bit error ratio versus signal-to-noise-ratio performance than the existing VLC-MIMO-OFDM systems that use the same number of transmit and receive units [LEDs and photo diodes (PDs)]. Compared with the single-input single-output (SISO) DC biased optical (DCO)-OFDM system, both spectral efficiency and DC bias can be doubled and removed respectively simply by exploiting a MIMO configuration.

Index Terms—Visible light communications (VLC), multiple-input-multiple-output (MIMO) systems, orthogonal frequency division multiplexing (OFDM), optical-spatial modulation (OSM), LED index modulation, maximum-a-posteriori probability (MAP) estimator.

I. Introduction

OPTICAL wireless communications (OWC) are an attractive new technology which has a great potential for the next generation wireless communications systems. Particularly, visible light communications (VLC) systems operating between the $400-800$ nm range could be the optimal solution for indoor mobile communications scenarios. This is due to the existing infrastructure, which can be reused and lighting and communication systems can be combined. Its distinct advantages such as license-free application, low deployment cost, wide bandwidth, energy efficiency and high security have made VLC one of the strongest candidates for beyond 5G wireless communications standards. Orthogonal frequency division multiplexing (OFDM) and its modified versions for intensity modulation/direct detection (IM/DD) systems in VLC have attracted significant attention due to frequency-selective behavior of the VLC channels for moderate and high data rates and the capability of easily achieving bit and power loading [1]. OFDM brings remarkable advantages in the presence of intersymbol interference (ISI) caused by frequency selectivity. However, since the transmitted signals are bipolar, it is impossible to transmit them without any modifications. Therefore, direct current (DC) bias addition and associated power inefficiency of optical OFDM constitute the main motivation behind the new energy efficient optical OFDM systems.

Utilization of the IM/DD technique inherently requires light intensity levels to be real and positive. These restrictions result in challenging problems when the goal is to transmit IM/DD signals and at the same time maintain the same spectral and power efficiency that the coherent transmission systems have. To address those challenges, many different methods have been proposed in the literature. For instance, real time-domain signals are directly obtained by using the conjugate symmetry property of the fast Fourier transformation (FFT), better known as the Hermitian symmetry. However, the main novelties of the proposed systems stem from how they deal with the bipolar nature of the signals. One of the straightforward solutions to obtain positive signals is to add a DC bias after the inverse FFT (IFFT) operation. The resulting system is called DC biased optical OFDM (DCO-OFDM) [2]. An elegant solution to the bipolarity problem is to use the FFT antisymmetry property that have led to asymmetrically clipped optical OFDM (ACO-OFDM) given in [3]. In ACO-OFDM, the DC bias is significantly reduced at the cost of sacrificing

half of the spectral efficiency. In [4], a novel unipolar transmission system, called U-OFDM, is proposed. The half-power (3 dB) penalty in ACO-OFDM caused by the time domain clipping is solved in U-OFDM by transmitting positive and negative frames separately; however, both systems achieve only half of the spectrum efficiency compared to DCO-OFDM. A new method proposed in [5] and [6], offers time domain superposition to achieve the same spectral efficiency as that of DCO-OFDM for both U-OFDM and ACO-OFDM. Recently, MIMO and index modulation transmission methods have started to attract significant attention in VLC literature to transmit additional bits with reduced energy consumption. In [7], MIMO-VLC based systems are investigated for multi-user case. Index modulation techniques, in which the indices of the building blocks of considered communications systems are used to transmit additional information bits, are particularly promising for energy and spectrum efficient IM/DD applications. Index modulation based transmission systems offer additional degree of freedom to compensate for the lose of the phase dimension [8]. In [9], spatial modulation (SM), which is the most common form of index modulation, is adopted for MIMO-VLC systems. The performance of the SM and some of its variants are investigated in [10] for VLC systems. Furthermore, a 2×2 optical SM based structure is proposed in [11] to solve the DC bias penalty issue by introducing two light emitting diodes (LEDs) to send negative and positive signals. Using the advantage of different wavelengths in the visible band is another promising solution to enhance the spectrum efficiency by means of multi-channel communication [12]–[16].

In this work, we propose two novel 4×4 MIMO-based optical OFDM systems for operation in the presence of frequency-flat and frequency-selective channels. These two schemes are called generalized LED index modulation optical OFDM (GLIM-OFDM) and extended GLIM-OFDM (e-GLIM-OFDM), respectively, where e-GLIM-OFDM is the modification of GLIM-OFDM to operate over frequency-selective VLC channels.

More specifically, the main contributions of the paper are summarized as follows:
- A novel 4×4 MIMO transmission-based technique, called GLIM-OFDM, is proposed. This scheme requires no Hermitian symmetry and DC bias to operate over frequency-flat VLC channels. In the proposed scheme, the real and imaginary parts of the complex time-domain OFDM signals are separated into their real and imaginary parts, and then these signals are transmitted over the MIMO-VLC channel by using the index modulation based on active LED indices. Higher spectral and power efficiencies are achieved by encoding the sign information of the complex signals to the location of transmit LEDs. Furthermore, a novel conditional maximum a posteriori probability (MAP) estimator is employed to estimate those real and imaginary parts of the OFDM signals at the receiver.
- A novel 4×4 MIMO transmission-based technique, called e-GLIM-OFDM, is also proposed by modifying the GLIM-OFDM structure. Similarly, this scheme requires

no Hermitian symmetry and DC bias to operate over frequency-selective VLC channels. Since it is not feasible to estimate directly the real and imaginary parts of the complex time-domain OFDM signals in this case, an efficient and feasible technique is proposed for the time-frequency domain transformations.
- Both analytical and computer software aided physical VLC channel models are obtained for three different scenarios: 1) Receivers located close to each other with a separation of 0.1 m, 2) Receivers are located apart with a separation of 0.8 m, 3) Receivers are aligned to their corresponding luminaries while the separation between receivers is 0.1 m. Physical VLC channel models including realistic source, detector and reflection parameters are obtained by a ray-tracing approach. Furthermore, the proposed scheme is also adopted for the frequency-selective VLC channels.
- Finally, it is shown that the proposed GLIM-OFDM and e-GLIM-OFDM schemes have superior bit error ratio (BER) performances as compared with the reference optical MIMO transmission systems.

The rest of the paper is organized as follows. In Section II, the system model for GLIM-OFDM is presented and the design of its receiver based on the conditional MAP estimator is introduced. In Sections III and IV, the design of e-GLIM-OFDM is given and both analytical and physical VLC channel modeling approaches are presented, respectively. Computer simulation results are provided in Section V and finally, conclusions are given in Section VI.

Notation: Throughout the paper, vectors are in bold lowercase letters and matrices are in bold capital letters. The transpose of a matrix/vector is expressed by $(.)^T$. Componentwise inequalities are given by $\preceq$ and $\succeq$. Complex and real normal distributions are given by $\mathcal{CN}(\mu, \sigma^2)$ and $\mathcal{N}(\mu, \sigma^2)$, respectively, where μ represents the mean and σ^2 represents the variance. $\mathbb{R}$ denotes the ring of real numbers. $N \times N$ FFT matrix is denoted by $\mathbf{F}$. Lastly, $\mathbf{0}$ and $[\mathbf{A}]_{m,n}$ are $N \times N$ zero matrix and (m, n)th element of a matrix $\mathbf{A}$, respectively.

II. GLIM-OFDM IN THE PRESENCE OF FREQUENCY-FLAT MIMO CHANNELS

The block diagram of the proposed GLIM-OFDM transceiver for frequency-flat MIMO channels is given in Fig. 1. $N \log_2(M)$ information bits carrying vector $\mathbf{u}$ enters the GLIM-OFDM transmitter for transmission of each OFDM block, where N is the number of OFDM subcarriers and M is the size of the considered signal constellation such as M-ary quadrature amplitude modulation (M-QAM). The DCO-OFDM, ACO-OFDM and non DC-biased OFDM (NDC-OFDM) schemes rely on Hermitian symmetry to produce real time-domain signals after the IFFT operation. In the proposed scheme, the OFDM modulator directly processes the complex frequency-domain OFDM frame $\mathbf{x}_F$ without requiring Hermitian symmetry. The resulting time-domain OFDM frame $\mathbf{x}_T = \begin{bmatrix} x_1 & \cdots & x_N \end{bmatrix}^T$ cannot be conveyed through a VLC channel because of its complex-valued and bipolar (positive and negative valued) elements. In order to solve this problem,
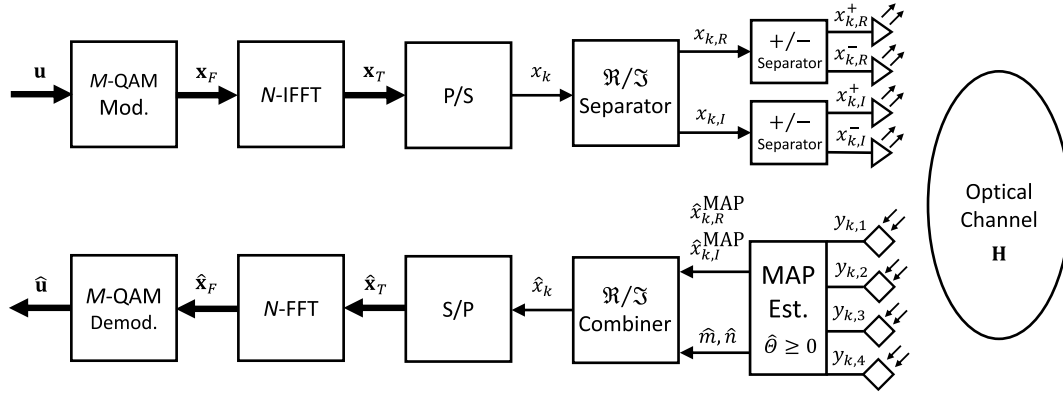
Fig. 1. Block diagram of the GLIM-OFDM scheme for a 4×4 MIMO-VLC system.

a new LED index modulation based MIMO transmission technique has been developed. After parallel-to-serial (P/S) conversion, using a similar technique as in [17] for each time-domain OFDM signal x_k, where $k = 0, 1, \ldots, N - 1$, first, the real and imaginary parts of the complex signal x_k are separated as $x_k = x_{k,R} + jx_{k,I}$. Then, the resulting real, but bipolar signals $x_{k,R}$ and $x_{k,I}$ are processed by positive-negative $(+/-)$ separators to obtain the following positive real-valued signals:

$$
x_{k,R}^+ = \begin{cases} x_{k,R} & \text{if } x_{k,R} > 0 \\ 0 & \text{if } x_{k,R} < 0 \end{cases} \quad x_{k,R}^- = \begin{cases} 0 & \text{if } x_{k,R} > 0 \\ -x_{k,R} & \text{if } x_{k,R} < 0 \end{cases}
$$
$$
x_{k,I}^+ = \begin{cases} x_{k,I} & \text{if } x_{k,I} > 0 \\ 0 & \text{if } x_{k,I} < 0 \end{cases} \quad x_{k,I}^- = \begin{cases} 0 & \text{if } x_{k,I} > 0 \\ -x_{k,I} & \text{if } x_{k,I} < 0. \end{cases}
$$
$$(1)$$

These signals can be transmitted simultaneously from an $n_R \times n_T$ MIMO VLC system, where n_R and n_T denote the number of receiver (Rx) and transmitter (Tx) units, respectively. It should be noted that, n_T must be divisible by four for the proposed scheme where it is taken as $n_T = 4$ in this work.

In the GLIM-OFDM scheme, LEDs transmit the absolute values of $x_{k,R}$ and $x_{k,I}$ signals and the index of the transmitting LED determines the sign of the corresponding signals similar to the NDC-OFDM scheme. However, unlike the NDC-OFDM, GLIM-OFDM completely avoids the Hermitian symmetry at the input of IFFT as well as the accompanying loss in spectral efficiency. Consequently, the spectral efficiency of the proposed scheme becomes $\log_2(M)$ [bits/s/Hz], which is twice that of NDC-OFDM and DCO-OFDM schemes, since Hermitian symmetry is no longer required to produce real-valued OFDM symbols.

The positive and real-valued OFDM time samples $x_{k,R}^+, x_{k,R}^-, x_{k,I}^+$ and $x_{k,I}^-$ are transmitted over the $n_R \times 4$ optical MIMO channel (represented by **H**) for $k = 0, 1, \ldots, N-1$ as

$$\mathbf{y} = \mathbf{Hx} + \mathbf{n} \tag{2}$$

where $\mathbf{y} = \begin{bmatrix} y_{k,1} & \cdots & y_{k,n_R} \end{bmatrix}^T \in \mathbb{R}^{n_R \times 1}$ is the vector of received signals that contains the electrical signals obtained from PDs at the Rx units. In (2), $\mathbf{n} \in \mathbb{R}^{n_R \times 1}$ is the vector of real-valued

additive white Gaussian noise (AWGN) samples, that models the shot noise and thermal noise. The elements of **n** follows $\mathcal{N}\left(0, \sigma_w^2\right)$ distribution, and are added to the received signals in the electrical domain. The transmitted signal vector $\mathbf{x} \in \mathbb{R}^{4 \times 1}$ is formed for GLIM-OFDM as

$$\mathbf{x} = \begin{bmatrix} x_{k,R}^+ & x_{k,R}^- & x_{k,I}^+ & x_{k,I}^- \end{bmatrix}^T \tag{3}$$

where the signals emitted by the LEDs are indicated by the elements of **x**. According to (1), for a given OFDM signal, only two out of four elements of **x** are non-zero, i.e., two LEDs are active (emitting light), while the other two LEDs remain inactive (turned off). As an example, for $x_k = -2.1 + j3.8$, we have $\mathbf{x} = \begin{bmatrix} 0 & 2.1 & 3.8 & 0 \end{bmatrix}^T$, i.e., the second LED is active and it transmits the absolute value of the real part of x_k and the third LED is also active for the transmission of the imaginary part of x_k, which is positive. In this way, the proposed scheme utilizes the index modulation concept for the active LED indices to transmit the complex OFDM signals.

In this study, we consider $n_R = 4$ for ease of presentation, while a generalization is straightforward. We assume that the LEDs are operating within their dynamic range. Note that the operation in (1) is not subject to non-linear distortions.

The 4×4 optical MIMO channel is represented by

$$\mathbf{H} = \begin{bmatrix} h_{1,1} & h_{1,2} & h_{1,3} & h_{1,4} \\ h_{2,1} & h_{2,2} & h_{2,3} & h_{2,4} \\ h_{3,1} & h_{3,2} & h_{3,3} & h_{3,4} \\ h_{4,1} & h_{4,2} & h_{4,3} & h_{4,4} \end{bmatrix} \tag{4}$$

where $h_{r,t}$ denotes the channel gain of the optical wireless link between the Tx unit (LED) t and the Rx unit (PD) r, where $(t, r) \in \{1, 2, 3, 4\}$. In this study, we consider the average electrical signal-to-noise ratio ($\mathrm{SNR_{Rx}}$) at the receiver as given in [18]–[20]:

$$\mathrm{SNR_{Rx}} = \frac{P_{\mathrm{Rx}}^{\mathrm{elec}}}{\sigma_n^2} = \frac{1}{\sigma_n^2} \zeta \left(P_{\mathrm{Rx}}^{\mathrm{opt}} \right)^2 \tag{5}$$

where ζ is the electrical-to-optical conversion factor that is taken as unity and $P_{\mathrm{Rx}}^{\mathrm{elec}}$ is the average received electrical power. The average received optical power can be expressed as,

$$P_{\mathrm{Rx}}^{\mathrm{opt}} = \frac{1}{n_R} \sum\nolimits_{r=1}^{n_R} \sum\nolimits_{t=1}^{n_T} h_{r,t} I \tag{6}$$

where I represents the mean optical intensity being emitted. Let us assume that $E\left\{\mathbf{x}_F^H \mathbf{x}_F\right\} = N$, i.e., M-QAM constellation is normalized to have unit-energy symbols. It can be shown that if the inverse fast Fourier transform (IFFT) operation satisfies the normalization of $E\left\{\mathbf{x}_T^H \mathbf{x}_T\right\} = N$, the elements of $\mathbf{x}_T$ follow $\mathcal{CN}(0, 1)$ distribution for large N values. Considering that $x_{k,R}$ and $x_{k,I} \sim \mathcal{N}(0, 1/2)$, due to the symmetry, all four elements of $\mathbf{x}$ have the following clipped Gaussian probability density function (p.d.f.)

$$p_{x_{k,R(I)}^{\pm}}(v) = \frac{1}{\sqrt{\pi}} e^{-v^2} u(v) + \frac{1}{2}\delta(v) \qquad (7)$$

where $u(v)$ and $\delta(v)$ denote the unit step and Dirac delta functions, respectively. Then, the average electrical power emitted from the one LED of GLIM-OFDM scheme is obtained as,

$$I = E\{x_{k,R(I)}^{\pm}\} = \int_0^{\infty} v p_{x_{k,R(I)}^{\pm}}(v)dv = 1/(2\sqrt{\pi}). \qquad (8)$$

A. Conditional MAP Estimator of GLIM-OFDM

The transmission model given in (2) resembles that of the classical single-carrier MIMO-SM systems; however, it differs from those models for two main reasons: Firstly, the received signals are real in (2) and secondly, the transmitted data vector $\mathbf{x}$ has a clipped Gaussian distribution. Furthermore, it is not possible to forward the received signal vector $\mathbf{y}$ to the OFDM demodulator directly, due to the fact that complex valued signals must be constructed first to obtain the estimate of the frequency domain OFDM block $\mathbf{x}_F$. A straightforward solution to the estimation problem formulated in (2) is the use of the zero-forcing (ZF) equalizer, which yields an estimate of $\mathbf{x}$ simply as

$$\hat{\mathbf{x}}^{ZF} = \mathbf{H}^{-1}\mathbf{y}. \qquad (9)$$

After this operation, the receiver can determine the indices of the active LEDs and corresponding signals by selecting the higher magnitude signals from $\hat{\mathbf{x}}^{ZF}$ [11]. Despite its simplicity, the ZF estimator can significantly enhance the noise power through multiplication of $\mathbf{n}$ with $\mathbf{H}^{-1}$; furthermore, it does not consider the probability distribution of $\mathbf{x}$ as a *a priori* information and consequently, it may produce negative-valued estimates. To overcome the aforementioned drawbacks of the ZF estimator, in this section, we propose a novel MAP estimator for the GLIM-OFDM scheme by taking into account the prior information we have for the signal vector $\mathbf{x}$.

The channel matrix $\mathbf{H}$ is defined in terms of its column vectors as $\mathbf{H} = \begin{bmatrix} \mathbf{h}_1 & \mathbf{h}_2 & \mathbf{h}_3 & \mathbf{h}_4 \end{bmatrix}$ and the observed signals given in (2) can be rewritten as

$$\mathbf{y} = \mathbf{h}_m \bar{x}_{k,R} + \mathbf{h}_n \bar{x}_{k,I} + \mathbf{n} \qquad (10)$$

where $\bar{x}_{k,R} = |x_{k,R}|$, $\bar{x}_{k,I} = |x_{k,I}|$, $m \in \{1, 2\}$ and $n \in \{3, 4\}$. It can be easily shown that $\bar{x}_{k,R}$ and $\bar{x}_{k,I}$ have a folded Gaussian (half-normal) distribution having the following p.d.f

$$p_{\bar{x}_{k,R(I)}}(v) = \frac{2}{\sqrt{\pi}} e^{-v^2} u(v). \qquad (11)$$

Consequently, for a given pair (m, n), the conditional MAP estimates of $\bar{x}_{k,R}$ and $\bar{x}_{k,I}$ can be obtained as

$$\left(\tilde{x}_{k,R}^{(m,n)}, \tilde{x}_{k,I}^{(m,n)}\right) = \arg\max_{\bar{x}_{k,R}, \bar{x}_{k,I}} p\left(\bar{x}_{k,R}, \bar{x}_{k,I} \mid \mathbf{y}\right) \qquad (12)$$

where $p\left(\bar{x}_{k,R}, \bar{x}_{k,I} \mid \mathbf{y}\right)$ is the p.d.f. of $\bar{x}_{k,R}$ and $\bar{x}_{k,I}$, conditioned on $\mathbf{y}$. After simple manipulations, (12) could be written as

$$\left(\tilde{x}_{k,R}^{(m,n)}, \tilde{x}_{k,I}^{(m,n)}\right) = \arg\min_{\bar{x}_{k,R}, \bar{x}_{k,I}} M^{MAP}(m, n, \bar{x}_{k,R}, \bar{x}_{k,I}). \qquad (13)$$

where $M^{MAP}\left(m, n, \bar{x}_{k,R}, \bar{x}_{k,I}\right)$ is the MAP estimation metric defined as

$$M^{MAP}\left(m, n, \bar{x}_{k,R}, \bar{x}_{k,I}\right) = \left\| \mathbf{y} - \mathbf{h}_m \bar{x}_{k,R} - \mathbf{h}_n \bar{x}_{k,I} \right\|^2 + 2\sigma_w^2 \left(\bar{x}_{k,R}^2 + \bar{x}_{k,I}^2\right). \qquad (14)$$

Using $\|\mathbf{a}\| = \mathbf{a}^T \mathbf{a}$ and after some algebra, (14) can be simplified as

$$M^{MAP}\left(m, n, \bar{x}_{k,R}, \bar{x}_{k,I}\right) = A\bar{x}_{k,R}^2 + B\bar{x}_{k,I}^2 + C\bar{x}_{k,R} + D\bar{x}_{k,I} + E\bar{x}_{k,R}\bar{x}_{k,I} \qquad (15)$$

where

$$\begin{aligned} A &= \mathbf{h}_m^T \mathbf{h}_m + 2\sigma_w^2 & B &= \mathbf{h}_n^T \mathbf{h}_n + 2\sigma_w^2 \\ C &= -2\mathbf{y}^T \mathbf{h}_m & D &= -2\mathbf{y}^T \mathbf{h}_n \\ E &= 2\mathbf{h}_m^T \mathbf{h}_n. \end{aligned} \qquad (16)$$

Taking the derivative of $M^{MAP}(m, n, \bar{x}_{k,R}, \bar{x}_{k,I})$ with respect to $\bar{x}_{k,R}$ and $\bar{x}_{k,I}$ and equating to zero yields the MAP estimates for $\bar{x}_{k,R}$ and $\bar{x}_{k,I}$, conditioned on (m, n), as

$$\tilde{x}_{k,R}^{(m,n)} = \left[\frac{2BC - ED}{E^2 - 4AB}\right]^+, \quad \tilde{x}_{k,I}^{(m,n)} = \left[\frac{2AD - EC}{E^2 - 4AB}\right]^+. \qquad (17)$$

where $[x]^+ := \max([0, x])$. Note that the optimal estimates of $\mathbf{q}$ in (17) also guarantee that $\tilde{x}_{k,R}^{(m,n)} \geq 0$ and $\tilde{x}_{k,I}^{(m,n)} \geq 0$ for all $\mathbf{Q}$ and $\mathbf{b}$, i.e. regardless of the SNR and the channel conditions.

In order to determine the indices of the active LEDs (i.e., estimations of m and n) as well as the corresponding estimates of $\bar{x}_{k,R}$ and $\bar{x}_{k,I}$, the conditional MAP estimator determines $\tilde{x}_{k,R}^{(m,n)}$ and $\tilde{x}_{k,I}^{(m,n)}$ for all possible (m, n) pairs, and then obtains the unconditional (actual) estimates of $\bar{x}_{k,R}$ and $\bar{x}_{k,I}$ as follows:

$$(\hat{m}, \hat{n}) = \arg\min_{m,n} M^{MAP}\left(m, n, \tilde{x}_{k,R}^{(m,n)}, \tilde{x}_{k,I}^{(m,n)}\right),$$

$$\text{where } \hat{x}_{k,R}^{MAP} = \tilde{x}_{k,R}^{(\hat{m},\hat{n})}, \quad \hat{x}_{k,I}^{MAP} = \tilde{x}_{k,I}^{(\hat{m},\hat{n})}. \qquad (18)$$

In other words, after the calculation of the MAP estimates of $\bar{x}_{k,R}$ and $\bar{x}_{k,I}$ for all $(m, n) \in \{(1, 3), (1, 4), (2, 3), (2, 4)\}$ that considers all possible active LED scenarios, the conditional MAP estimator of the GLIM-OFDM scheme decides on the most likely active LED pair $(\hat{m}, \hat{n})$ and corresponding estimates of $\bar{x}_{k,R}$ and $\bar{x}_{k,I}$ $(\hat{x}_{k,R}^{MAP}, \hat{x}_{k,I}^{MAP})$ by calculating the MAP estimation metric given by (14) for all four scenarios.

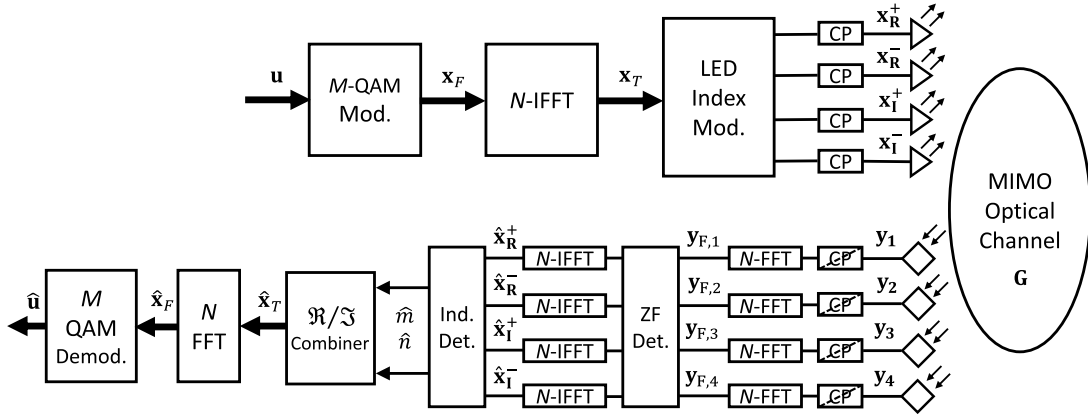Fig. 2. Block Diagram of the extended GLIM-OFDM Scheme for a 4×4 frequency-selective MIMO VLC channels

---

Algorithm 1 Conditional MAP Estimator

1: **for** $m = 1 : 2$ **do**
2:    **for** $n = 3 : 4$ **do**
3:       Estimate, $\tilde{x}_{k,R}^{(m,n)}$ and $\tilde{x}_{k,I}^{(m,n)}$ values from (17)
4:       Estimate, $(\tilde{m}, \tilde{n})$ indices from (18)
5:    **end for**
6: **end for**
7: Combination of symbols: $\pm \tilde{x}_{k,R}^{(\tilde{m},\tilde{n})} \pm j \tilde{x}_{k,I}^{(\tilde{m},\tilde{n})}$ via $(\tilde{m}, \tilde{n})$.

The $\Re/\Im$ combiner then calculates the estimate of the complex OFDM signal x_k as

$$\hat{x}_{k,R} = \begin{cases} \hat{x}_{k,R}^{\text{MAP}}, & \text{if } m = 1 \\ -\hat{x}_{k,R}^{\text{MAP}}, & \text{if } m = 2 \end{cases} \quad \hat{x}_{k,I} = \begin{cases} \hat{x}_{k,I}^{\text{MAP}}, & \text{if } n = 3 \\ -\hat{x}_{k,I}^{\text{MAP}}, & \text{if } n = 4 \end{cases}$$

$$(19)$$

In Algorithm 1, we summarize the steps of the proposed MAP estimator. After this point, classical OFDM processing steps such serial-to-parallel (S/P) conversion, FFT and M-ary demodulation are applied to obtain the estimate $\hat{\mathbf{u}}$ of the information bit vector $\mathbf{u}$.

B. Calculation of Mean Square Error

Given the estimates $(\hat{m}, \hat{n})$ of the indices of the active LEDs for $k = 0, 1, \cdots, N - 1$ and assuming that they are correct, we now derive the mean-square error (MSE) for the estimates of $\mathbf{q} = [\bar{x}_{k,R} \ \bar{x}_{k,I}]^T$ defined as

$$\text{MSE}_{\mathbf{y},\mathbf{q}} = E\{\boldsymbol{\varepsilon}^T \boldsymbol{\varepsilon}\}$$

where $\boldsymbol{\varepsilon}$ represents the error vector, $\boldsymbol{\varepsilon} = \mathbf{q} - \hat{\mathbf{q}}^{(\hat{m},\hat{n})}$ and $\hat{\mathbf{q}} \equiv \hat{\mathbf{q}}^{(\hat{m},\hat{n})} = [\hat{x}_{k,R} \ \hat{x}_{k,I}]^T$. As can be seen from (10) and (17), $\hat{\mathbf{q}}$ depends linearly on $\mathbf{y}$ and the elements of the $\hat{\mathbf{q}}$ are jointly Gaussian distributed. Consequently, $\boldsymbol{\varepsilon}$ is also Gaussian with zero mean and its covariance matrix is given as [21]:

$$\mathbf{C}^{(\hat{m},\hat{n})} = \left(\frac{1}{\sigma_q^2} \mathbf{I} + \frac{1}{\sigma_n^2} \hat{\mathbf{H}}^T \hat{\mathbf{H}} \right)^{-1} \in \mathbb{R}^{2 \times 2} \qquad (20)$$

where $\hat{\mathbf{H}} = \begin{bmatrix} \mathbf{h}_{\hat{m}} & \mathbf{h}_{\hat{n}} \end{bmatrix} \in \mathbb{R}^{n_R \times 2}$ and $\sigma_q^2 = \sigma_{\bar{x}_{k,R(I)}}^2$ is the variance of the prior density of $\bar{x}_{k,R(I)}$.

It can be easily shown from (11) that $\sigma_q^2 = \frac{\pi - 1}{4\pi}$. Finally, for $k = 0, 1, \cdots, N - 1$, the MSE values of the estimates, $\tilde{x}_{k,R}^{(\hat{m},\hat{n})}$ and $\tilde{x}_{k,I}^{(\hat{m},\hat{n})}$ are equal to the diagonal elements of the error covariance matrix, namely,

$$\text{MSE}\left(\tilde{x}_{k,R}^{(\hat{m},\hat{n})}\right) = [\mathbf{C}^{(\hat{m},\hat{n})}]_{1,1}$$

$$\text{MSE}\left(\tilde{x}_{k,I}^{(\hat{m},\hat{n})}\right) = [\mathbf{C}^{(\hat{m},\hat{n})}]_{2,2}. \qquad (21)$$

Finally the average MSE for $\hat{\mathbf{x}}_{R(I)} = [\hat{x}_{0,R(I)}, \hat{x}_{1,R(I)}, \cdots, \hat{x}_{0,R(I)}]^T$ can be obtained as follows,

$$\overline{\text{MSE}}\left(\hat{x}_{R(I)}\right) = \frac{1}{N} \sum_{k=0}^{N-1} \text{MSE}\left(\tilde{x}_{k,R(I)}^{(\hat{m},\hat{n})}\right). \qquad (22)$$

In Section V, using the calculated MSE values in (22), we present both analytical and computer simulation error performance of the MAP estimator for the GLIM-OFDM scheme.

III. GLIM-OFDM IN THE PRESENCE OF FREQUENCY-SELECTIVE MIMO CHANNELS

In this section, we propose a novel design for the GLIM-OFDM, which is called extended GLIM-OFDM (e-GLIM-OFDM) and suitable for the frequency-selective MIMO visible light channels. It is already known that frequency responses of the front-end devices limits the data rates of the system. However, as data rate gets higher, multipath characteristics of the channel becomes more dominant, resulting in ISI. On the other hand, OFDM is known to be an efficient technique to cope with the multi-path channel effects. However, MIMO frequency selectivity for VLC channels is a quite new concept and to the best of authors' knowledge, e-GLIM-OFDM design and its performance in the presence of frequency-selective MIMO channel model are investigated for the first time in the literature. Block diagram of the e-GLIM-OFDM scheme is given in Fig. 2. Unlike the GLIM-OFDM scheme for flat VLC channels, after performing LED index modulation, the time-domain OFDM frame $\mathbf{x}_T$ is

extended into four vectors and a cyclic prefix is appended to the beginning of each transmission vector. Accordingly, each luminary here transmits its own data vector, which corresponds to a part of the overall transmitted vector, $\boldsymbol{\lambda}_{\mathbf{CP}} = [\mathbf{x}_R^+ \ \mathbf{x}_R^- \ \mathbf{x}_I^+ \ \mathbf{x}_I^-]^T \in \mathbb{R}^{4(N+L_{cp}) \times 1}$ where $\mathbf{x}_R^+$, $\mathbf{x}_R^-$, $\mathbf{x}_I^+$, $\mathbf{x}_I^-$ are the $(N + L_{cp}) \times 1$ real-valued vectors after the insertion of CP. For the sake of simplicity, a 4×4 system is considered in this work. However, the extension to higher MIMO systems can be easily performed. At the receiver side, $(N + L_{cp}) \times 1$ real-valued received signal vectors are obtained from each of the PDs as, $\mathbf{y}_i$ where $i \in \{1, 2, 3, 4\}$. The overall received vector, $\boldsymbol{\psi}_{\mathbf{CP}} = [\mathbf{y}_1 \ \mathbf{y}_2 \ \mathbf{y}_3 \ \mathbf{y}_4]^T \in \mathbb{R}^{4(N+L_{cp}) \times 1}$, can be expressed as

$$\mathbf{y}_1 = \mathbf{x}_R^+ \circledast \mathbf{g}_{1,1} + \mathbf{x}_R^- \circledast \mathbf{g}_{1,2} + \mathbf{x}_I^+ \circledast \mathbf{g}_{1,3} + \mathbf{x}_I^- \circledast \mathbf{g}_{1,4} + \boldsymbol{\rho}_1$$

$$\mathbf{y}_2 = \mathbf{x}_R^+ \circledast \mathbf{g}_{2,1} + \mathbf{x}_R^- \circledast \mathbf{g}_{2,2} + \mathbf{x}_I^+ \circledast \mathbf{g}_{2,3} + \mathbf{x}_I^- \circledast \mathbf{g}_{2,4} + \boldsymbol{\rho}_2$$

$$\mathbf{y}_3 = \mathbf{x}_R^+ \circledast \mathbf{g}_{3,1} + \mathbf{x}_R^- \circledast \mathbf{g}_{3,2} + \mathbf{x}_I^+ \circledast \mathbf{g}_{3,3} + \mathbf{x}_I^- \circledast \mathbf{g}_{3,4} + \boldsymbol{\rho}_3$$

$$\mathbf{y}_4 = \mathbf{x}_R^+ \circledast \mathbf{g}_{4,1} + \mathbf{x}_R^- \circledast \mathbf{g}_{4,2} + \mathbf{x}_I^+ \circledast \mathbf{g}_{4,3} + \mathbf{x}_I^- \circledast \mathbf{g}_{4,4} + \boldsymbol{\rho}_4$$

$$(23)$$

where $\circledast$ is the circular convolution operation, $\mathbf{g}_{r,t}$ is the $k \times 1$ frequency-selective channel coefficients vector between t^{th} LED and r^{th} PD and $\boldsymbol{\rho}_i$'s are $(N + L_{cp}) \times 1$ dimensional real-valued AWGN vectors. After computing FFT of the CP removed received signal vector $\boldsymbol{\psi}$, the circular convolution operation could be converted into matrix multiplication as,

$$\boldsymbol{\Omega}\boldsymbol{\psi} = \mathbf{G} \cdot \boldsymbol{\Omega}\boldsymbol{\lambda} + \boldsymbol{\Omega}\boldsymbol{\gamma} \qquad (24)$$

where $\boldsymbol{\Omega}$ is the $4N \times 4N$ diagonal FFT matrix, which could be given as,

$$\boldsymbol{\Omega} = \begin{bmatrix} \mathbf{F} & \mathbf{0} & \mathbf{0} & \mathbf{0} \\ \mathbf{0} & \mathbf{F} & \mathbf{0} & \mathbf{0} \\ \mathbf{0} & \mathbf{0} & \mathbf{F} & \mathbf{0} \\ \mathbf{0} & \mathbf{0} & \mathbf{0} & \mathbf{F} \end{bmatrix}$$

and $\mathbf{G}$ is a $4N \times 4N$ sized complex matrix whose elements are $\mathbf{G}_{r,t} = \mathrm{diag}(\mathbf{F}\mathbf{g}_{r,t})$ and $\boldsymbol{\gamma}_{\mathbf{CP}} = [\boldsymbol{\rho}_1 \ \boldsymbol{\rho}_2 \ \boldsymbol{\rho}_3 \ \boldsymbol{\rho}_4]^T$ is the $4(N + L_{cp}) \times 1$ dimensional complex AWGN vector. Basic ZF equalization performed in the frequency-domain as,

$$\boldsymbol{\psi}^{ZF} = \mathbf{G}^{-1} \cdot \boldsymbol{\Omega}\boldsymbol{\psi} = \boldsymbol{\Omega}\boldsymbol{\lambda} + \mathbf{G}^{-1}\boldsymbol{\Omega}\boldsymbol{\gamma}. \qquad (25)$$

After performing IFFT for the each stream individually, we can obtain the estimates of the transmission vectors and easily determine the indices of the active LEDs by comparing the corresponding elements of $(\mathbf{x}_R^+, \mathbf{x}_R^-)$ and $(\mathbf{x}_I^+, \mathbf{x}_I^-)$ vector pairs for each subcarrier. Error performance of the proposed system in the presence frequency-selective channels is investigated in Section V.

IV. PHYSICAL VLC CHANNEL MODELS

Determining the channel impulse response (CIR) in VLC systems is a challenging task since the received power is closely related to the channel link design. We want that the loss incurred in the optical channel is to be made as small as possible as in an effort to reduce the transmission power and to facilitate the use of simple and low-power receivers. To evaluate the received power, a commonly deployed VLC channel

model in earlier works [22]–[24] focuses on scenarios where channel gains are obtained with a limited number of reflections (i.e., up to second order) specifically considering zero order reflections (i.e., line-of-sight (LOS) response). In these studies, the analytical channel gains can be expressed as

$$h_{r,t}$$
$$= \begin{cases} \dfrac{(m+1) A_r R_p}{2\pi d_{r,t}^2} \cos^m \left(\phi_{r,t}\right) \cos \left(\psi_{r,t}\right), & 0 \leq \psi_{r,t} \leq \Psi_{1/2} \\ 0, & \psi_{r,t} > \Psi_{1/2} \end{cases}$$
$$(26)$$

where A_r denotes the photo-detector (PD) area, $d_{r,t}$ denotes the distance between the corresponding LED and PD pair, R_p is the responsivity of the PD and assumed to be unity in this study. Additionally, $\phi_{r,t}$ and $\psi_{r,t}$ represent the angle of irradiance and the angle of incidence, respectively, and $m = -\ln 2 / \ln(\cos \Phi_{1/2})$ is the order of Lambertian emission, where $\Phi_{1/2}$ denotes the semi-angle of the LED. $\Psi_{1/2}$ is the field-of-view (FOV) semiangle of the PD. Since the effect of higher order reflections is not taken into account in (26), the received power is underestimated in this model.

The above channel model is limited to the assumption of a Lambertian source and does not take into account the effect of reflections. Hence, a physical channel modeling approach is adopted in [1] that utilizes the ray-tracing based approaches. Ray-tracing takes the characteristics of propagation environment (i.e., presence of human beings, objects, etc), light sources (i.e., beamform) and detectors (i.e., rotation, field-of-view etc) into account precisely.

A. Frequency-Flat MIMO VLC Channels

In this study, we consider a 4×4 MIMO-VLC system that is operating in a $5 \ \mathrm{m} \times 5 \ \mathrm{m} \times 3 \ \mathrm{m}$ typical room as illustrated in Fig. 3 with plaster ceiling/walls and a pinewood floor. We model the table as a CAD object with coating material of pinewood. We assume four luminaries on the ceiling with equidistant spacing of 2 m. In [25], the ideal case of 100 LED chips per each luminary is considered, while by taking advantage of the simplification method [26], less number of LED chips can be used to achieve the same channel parameters. Based on [26], we adopt the configuration in which a LED luminary array with the size of 0.6 m × 0.6 m is employed consisting of 9 LED chips and each LED chip radiates 5 W with a view angle of 120°. This satisfies the typical illumination levels for office environment [27]. The field-of-view (FOV) semi-angle and area of the PD are 85°and 1 cm², respectively. The PDs are located at a height of 0.8 m, which is the standard height of a table. Coordinates of the luminaries and PDs are given in Table I for two different configurations named as Config A (PDs are in the center of the table with equidistant spacing of 0.1 m) and Config B (PDs are at the corners of the table with equidistant spacing of 0.8 m). Luminaries and PDs are assumed to be facing vertically downward to the floor and upward to the ceiling, respectively.

Based on the given scenarios and by taking advantage of the advanced ray tracing features of the optical design
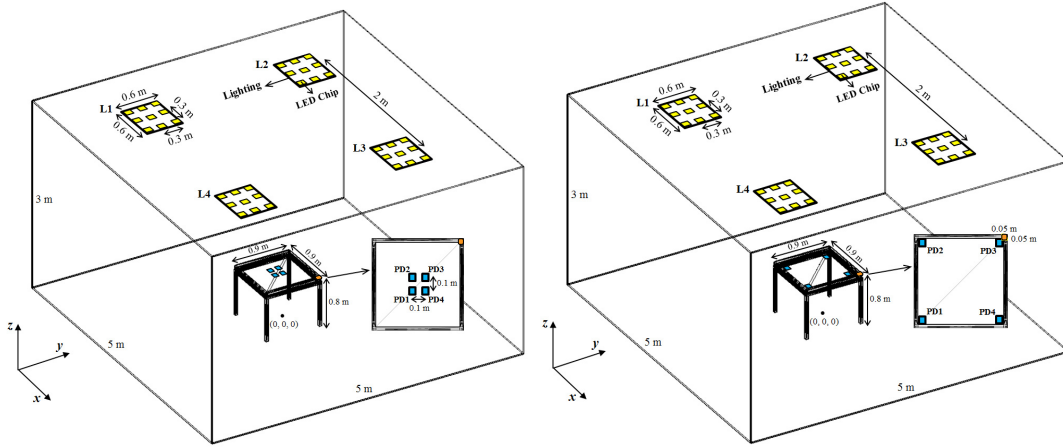
Fig. 3.   Configuration A (Receivers in the center of the table) and B (Receivers at the corners of the table).

TABLE I

PHYSICAL PARAMETERS OF THE SIMULATION ENVIRONMENT

Parameters	Values
Dimensions of the Room (W × L × H)	5 m × 5 m × 3 m
Number of Luminaries	4
Number of LED Chips per Luminary	9
Model of LED Chips	Cree Xlamp MC-E White
Power of LED Chips	5 W
Luminary (L) Positions (x, y, z) (m)	L1: (-1.3, -0.7, 3) L2: (-1.3, 1.3, 3) L3: (0.7, 1.3, 3) L4: (0.7, -0.7, 3)
Photodetector (PD) Positions (x, y, z) (m)	Conf A: PD1: (-0.05, -0.05, 0.8) PD2:(-0.05, 0.05, 0.8)
	PD3: (0.05, 0.05, 0.8) PD4: (0.05, -0.05, 0.8)
	Conf B: PD1: (-0.4, -0.4, 0.8) PD2: (-0.4, 0.4, 0.8)
	PD3: (0.4, 0.4, 0.8) PD4: (0.4, -0.4, 0.8)
Viewing angle of Luminary	120°
FOV semiangle of PD (degrees)	85°
Area of PD	1 cm²
Materials	Walls & Ceiling: Plaster
	Floor & Desk: Pine Wood

software, we calculate the detected power and path lengths from source to detector for each ray. These parameters are used to obtain the CIRs between each luminary and PD, and expressed as [1]

$$h(t) = \sum_{i=1}^{N_r} P_i \delta(t - \tau_i) \qquad (27)$$

where P_i is the optical power of the ith ray, τ_i is the propagation time of the ith ray and N_r is the number of rays received at the detector. Once we obtain CIRs, the fundamental channel parameters can be computed. Truncation time (T_{tr}) is defined as

$$\int_0^{T_{tr}} h(t)dt = 0.97 \int_0^\infty h(t)dt \qquad (28)$$

which denotes the region of CIR with the most energy concentrated. While the above formula assumes 97 % of the total energy in the calculation, other percentages can be also chosen based on the application. Channel DC gain (H_0), root-mean-square (RMS) delay spread (τ_{RMS}) and mean delay spread (τ_0) are also important parameters of a VLC channel,

which can be defined as [28],

$$H_0 = \int_0^\infty h(t)dt,$$

$$\tau_{RMS} = \sqrt{\frac{\int_0^\infty (t - \tau_0)^2 h(t)dt}{\int_0^\infty h(t)dt}},$$

$$\tau_0 = \frac{\int_0^\infty t \cdot h(t)dt}{\int_0^\infty h(t)dt}. \qquad (29)$$

The analytical channel gains for Configs A and B by considering the parameters given in the Table I are calculated respectively as follows:

$$\mathbf{H}_A^a \approx 10^{-5} \times \begin{pmatrix} 0.3489 & 0.3288 & 0.3104 & 0.3288 \\ 0.3288 & 0.3489 & 0.3288 & 0.3104 \\ 0.3104 & 0.3288 & 0.3489 & 0.3288 \\ 0.3288 & 0.3104 & 0.3288 & 0.3489 \end{pmatrix}$$

$$\mathbf{H}_B^a \approx 10^{-5} \times \begin{pmatrix} 0.4984 & 0.3005 & 0.2008 & 0.3005 \\ 0.3005 & 0.4984 & 0.3005 & 0.2008 \\ 0.2008 & 0.3005 & 0.4984 & 0.3005 \\ 0.3005 & 0.2008 & 0.3005 & 0.4984 \end{pmatrix}.$$

Similarly, physical indoor VLC channel gains obtained for Configs A and B by using our methodology and given parameters in Table I are as

$$\mathbf{H}_A^p \approx 10^{-5} \times \begin{pmatrix} 0.4866 & 0.4822 & 0.4533 & 0.4822 \\ 0.4822 & 0.4866 & 0.4822 & 0.4533 \\ 0.4533 & 0.4822 & 0.4866 & 0.4822 \\ 0.4822 & 0.4533 & 0.4822 & 0.4866 \end{pmatrix}$$

$$\mathbf{H}_B^p \approx 10^{-5} \times \begin{pmatrix} 0.6533 & 0.3955 & 0.3066 & 0.3955 \\ 0.3955 & 0.6533 & 0.3955 & 0.3066 \\ 0.3066 & 0.3955 & 0.6533 & 0.3955 \\ 0.3955 & 0.3066 & 0.3955 & 0.6533 \end{pmatrix}.$$

The channel parameters for $\mathbf{H}_A^p$ and $\mathbf{H}_B^p$ are summarized in Table II. It is observed that the channel gains obtained with the analytical method (i.e., LOS response) are smaller than those ones obtained by the physical method. As a result of this, we can take the effect of higher order reflections into consideration in our methodology. Since the detectors are

TABLE II

CHANNEL PARAMETERS FOR $\mathbf{H}_A^P$ AND $\mathbf{H}_B^P$

Channel Gain	Configuration A (Receivers in Center, $d_{Rx} = 0.1$ m)			Configuration B (Receivers at the Corners, $d_{Rx} = 0.8$ m)		
	T_{tr} (ns)	τ_0 (ns)	τ_{RMS} (ns)	T_{tr} (ns)	τ_0 (ns)	τ_{RMS} (ns)
$h_{1,1}$	40	14.22	10.18	37	12.40	8.98
$h_{1,2}$	40	14.44	9.79	40	15.22	10.40
$h_{1,3}$	40	14.52	9.84	42	17.28	11.23
$h_{1,4}$	40	14.44	9.79	40	15.22	10.40
$h_{2,1}$	40	14.44	9.79	40	15.22	10.40
$h_{2,2}$	40	14.22	10.18	37	12.40	8.98
$h_{1,3}$	40	14.44	9.79	40	15.22	10.40
$h_{2,4}$	40	14.52	9.84	42	17.28	11.23
$h_{3,1}$	40	14.52	9.84	42	17.28	11.23
$h_{3,2}$	40	14.44	9.79	40	15.22	10.40
$h_{3,3}$	40	14.22	10.18	37	12.40	8.98
$h_{3,4}$	40	14.44	9.79	40	15.22	10.40
$h_{4,1}$	40	14.44	9.79	40	15.22	10.40
$h_{4,2}$	40	14.52	9.84	42	17.28	11.23
$h_{4,3}$	40	14.44	9.79	40	15.22	10.40
$h_{4,4}$	40	14.22	10.18	37	12.40	8.98

TABLE III

COMPARISON OF MIMO SYSTEMS

Modulation	$n_R \times n_T$	Spectral Efficiency	Optical Power, $E\{x\}$	Complexity
GLIM-OFDM	4x4	$\sim \log_2 M$	$\frac{\sigma}{2\sqrt{\pi}}$	$\sim O(N \log_2 N)$
e-GLIM-OFDM	4x4	$\sim \log_2 M$	$\frac{\sigma}{2\sqrt{\pi}}$	$\sim O(N \log_2 N)$
OSM-DCO-OFDM	4x4	$\sim \frac{\log_2(M \cdot n_T)}{2}$	$\frac{\sigma}{\sqrt{2\pi}}exp(\frac{-B^2}{2\sigma^2}) + B(1 - Q(\frac{B}{\sigma}))$	$\sim O(N \log_2 N)$
OSM-ACO-OFDM	4x4	$\sim \frac{\log_2(M \cdot n_T)}{4}$	$\frac{\sigma}{4\sqrt{\pi}}$	$\sim O(N \log_2 N)$
V-BLAST-ACO OFDM	4x4	$\sim \log_2 M$	$\frac{\sigma}{2\sqrt{\pi}}$	$\sim O(N \log_2 N)$
NDC-OFDM	4x4	$\sim \log_2(M \cdot n_T)$	$\frac{\sigma}{\sqrt{2\pi}}$	$\sim O(N \log_2 N)$

placed at the corner sides of the table in Config B, they receive more scattering from walls and therefore, the difference of analytical and physical channel gains increases with respect to that one in Config A.

B. Obtaining Frequency-Selective MIMO VLC Channels

In this subsection, we explain the methodology to obtain the physical multi-path VLC channels. Environmental factors such as humans inside the room, furniture structure including coating material types, location of the objects and the sources/detectors play a vital role on reflection and refraction patterns. All of these material characteristics are taken into account for higher order reflections and frequency-selective CIRs are acquired by employing the same methodology as presented in the frequency-flat case.

For our investigations of the frequency-selective visible light channel models, we have used IEEE 802.15.7r1 reference channel models obtained for manufacturing cells [29]. In this configuration, six LEDs are located at the head of the robotic arm where they are located at the sides of a cubical package. Each face of the cube is equipped with one transmitter ensuring $360°$ of coverage. The LEDs are commercially available from Cree (MC-E) with non-ideal Lambertian pattern and a half viewing angle of $60°$. The FOV semi-angle and the area of the detector are $35°$ and 1 cm^2, respectively. Eight test points are also considered on the top of the cell boundaries. We select the CIRs between LED1, LED3, LED5 and LED6 as transmitters and D1, D3, D5 and D7 as receivers (i.e., placed at the corners of cell boundaries). It is observed that due to the delay difference in the VLC channels under consideration and the signaling rates higher than 100 Mbits/sec, the multipath components are resolvable and can be treated as multitap channel leading to the frequency-selective channels. The resulting CIRs obtained for this configuration are given in the Appendix.

For the sake of reality, the sampling frequency f_s for the channel is taken as 100 MHz where the sampling period is $T_s = 10$ ns. Since the maximum delay spread of the obtained channel is 60 ns, $L = 6$ taps frequency-selective VLC channel vectors are obtained by down-sampling. Length of the cyclic

prefix in Section III is also chosen as $L_{cp} = 6$ in computer simulations to make sure that it equals to the maximum delay spread of the channel.

V. COMPLEXITY ANALYSIS AND COMPUTER SIMULATIONS

In this section, we present computational complexity analyses as well as the computer simulations to perform comparisons with the reference schemes given in Table III.

A. Complexity Analysis

The details of the computational complexity of the proposed algorithm is presented in Table III. For the GLIM-OFDM receiver, to implement the conditional MAP algorithm for estimation of the real channel path gains in (16), it is necessary to compute only C and D in (17). Since the channel is deterministic and does not change with time, A, B and E can be precomputed and stored in the receiver. Hence, it can be easily checked that for all (m, n) pair where $m = 1, 2$ and $n = 3, 4$ for $k = 1, 2, \cdots, N$ values, $44N$ real multiplications (RM) and $16N$ real additions (RA)s are required. In addition, the computation of the MAP metric to determine the indices of the active LEDs requires $32N$ RM and $16N$ RA. On the other hand, OFDM algorithm with an FFT size of N requires approximately $4N \log_2(N)$ real operations (multiplications plus additions). Consequently, the overall complexity order in real operations for GLIM-OFDM is $76N + 4N \log_2(N)$ RM and $32 N + 4 \log_2(N)$ RA, which makes $\sim O(N \log_2 N)$.

To determine the computational complexity of e-GLIM-OFDM receiver, we refer to Fig. 2. Four N-FFT operations of the four received vectors ($\mathbf{y}_{F,k}$ for $k = 1, 2, 3, 4$), require approximately $16N \log_2(N)$ real operations. The implementation of the following ZF detector in Fig. 2 requires approximately $16N$ RM and $8 N$ RA. The main reason is that the overall frequency domain channel matrix $\mathbf{G} = [\mathbf{G}_{i,j}] \in \mathbb{R}^{4N \times 4N}$ is a 4×4 block matrix, in which each sub-block $\mathbf{G}_{i,j} \in \mathbf{G}$, for $i, j = 1, 2, 3, 4$ is a diagonal matrix. Since the channels are deterministic and known to the receiver, $\mathbf{G}$ as well as $\mathbf{G}^{-1}$ can be pre-computed and stored at the receiver. Hence, the only computational complexity in implementing the ZF detector comes from the multiplication of $\mathbf{G}^{-1}$ with the vector $\mathbf{y}_F = [\mathbf{y}_{F,1}, \ldots, \mathbf{y}_{F,4}]^T \in \mathbb{C}^{4N}$. Moreover, from matrix algebra, it is known that the inverse of $\mathbf{G}$ is also a 4×4 block diagonal matrix. This property simplifies the computational complexity
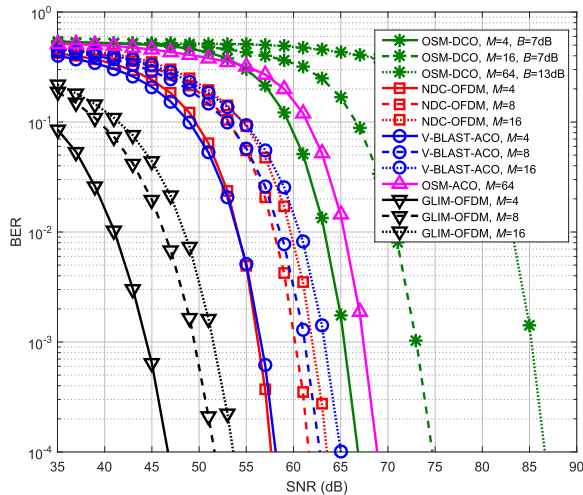
Fig. 4. BER performance comparison of optical MIMO-OFDM schemes for 2 (straight), 3 (dashed) and 4 (dotted) bits/s/Hz in analytic channel $\mathbf{H}_A^a$.
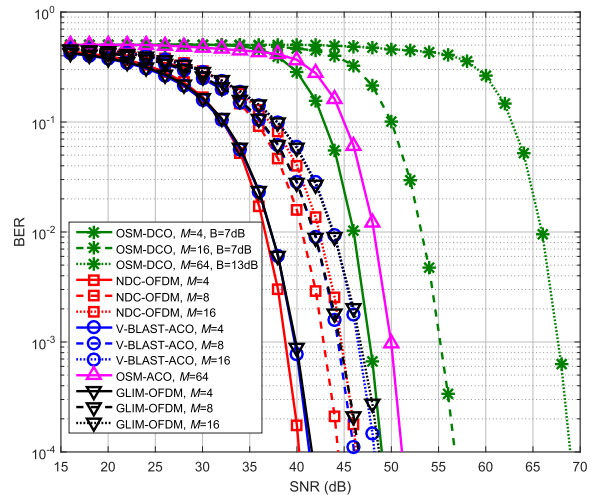

Fig. 5. BER performance comparison of optical MIMO-OFDM schemes for 2 (straight), 3 (dashed) and 4 (dotted) bits/s/Hz in physical channel $\mathbf{H}_A^p$.

substantially since the output of the ZF detector can simply be determined by four separated reduced-dimensional matrix multiplications. Thus, the computational complexity of the ZF detector is reduced from $\sim O(N^2)$ to $\sim O(N)$. After ZF detector, four IFFT operations, to transform the ZF detector output in the time-domain, requires again $16N \log_2(N)$ complex operations. After that, $32N$ RM and $16N$ RA operations are required to determine the indices of active LEDs and $4N \log_2(N)$ operations required for the FFT procedure. Therefore, the overall complexity order in real operations for e-GLIM-OFDM is $48N + 36 \log_2(N)$ RM and $24 N + 36 \log_2(N)$ RA, which makes $\sim O(N \log_2 N)$.

Computational complexities of the GLIM-OFDM and e-GLIM-OFDM schemes are compared with the reference VLC systems, such as parallel NDC-OFDM scheme, obtained by the parallel concatenation of two 2×2 NDC-OFDM schemes, [11], OSM-OFDM-ACO, OSM-OFDM-DCO schemes that are combining optical spatial modulation (OSM) concept [30] with optical OFDM [31] methodology, and vertical Bell Labs layered space-time (V-BLAST) type OFDM-ACO scheme [32] in Table III. When a similar complexity analysis is carried out for the above schemes, it is concluded that all the reference systems have asymptotically same complexity, namely, $\sim O(N \log_2 N)$, as shown in Table III.

B. Performance of GLIM-OFDM

In this subsection, we provide BER performance comparisons between the GLIM-OFDM scheme and the reference systems with respect to average received electrical SNR. Spectral efficiencies and optical powers of the reference systems are given in the Table III where B is the DC bias value for DCO-OFDM. In our comparisons, BER vs. SNR performance curves are presented for the spectral efficiency values of 2, 3 and 4 bit/sec/Hz in various VLC channel configurations, where the number of subcarriers is taken as $N = 256$.

TABLE IV
PEARSON'S CORRELATION COEFFICIENT VALUES
FOR CHANNEL CONFIGURATIONS

Channel Configuration	r
$\mathbf{H}_A^a$	0.0236
$\mathbf{H}_A^p$	0.0114
$\mathbf{H}_B^a$	0.1982
$\mathbf{H}_B^p$	0.1777
$\mathbf{H}_C^p$	0.3878

In Figs. 4 and 5, the BER performance of the proposed system is compared with other reference MIMO systems for the Config A ($d_{Tx} = 0.1$ m). It can be inferred from these figures that GLIM-OFDM outperforms the other reference systems in Fig. 4, whereas this is not the case indicated by the curves in Fig. 5. This can be explained as follows. The BER performance of the GLIM-OFDM system is highly dependent on the correlation between diagonal (LOS/direct) and off-diagonal (NLOS/indirect) elements of the channel matrix. It has excellent BER performance when the channel matrix is close to diagonal. Given the entries of the channel matrix, to determine how being "close" to the diagonal, a natural approach is to compute the correlation coefficient, r, between the rows and columns of the channel matrix. Strong correlation means that r is close to one and the matrix entries tend to be near the diagonal. This is also robust, since the correlation coefficient is unchanged if the channel matrix is scaled. The correlation values in Table IV show that the channel matrices of the different configurations considered in our computer simulations can be classified basically into three different channel structures. Such that, $\mathbf{H}_A^a$ and $\mathbf{H}_A^p$ have the weakest correlation values and consequently, they are far from being close to a diagonal matrix structure. On the other hand, as $\mathbf{H}_A^p$ and $\mathbf{H}_B^p$ can be considered having a modest diagonal structure, and the last channel matrix $\mathbf{H}_C^p$ in Table IV shows a strong diagonal structure.
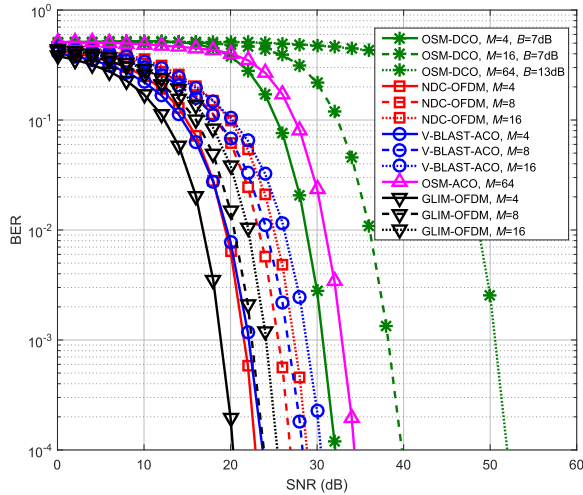
Fig. 6. BER performance comparison of optical MIMO-OFDM schemes for 2 (straight), 3 (dashed) and 4 (dotted) bits/s/Hz in analytic channel $\mathbf{H}_B^a$.

Fig. 8. Configuration C (Receivers are aligned to their correspondent LEDs to have stronger LOS link with a less correlation).
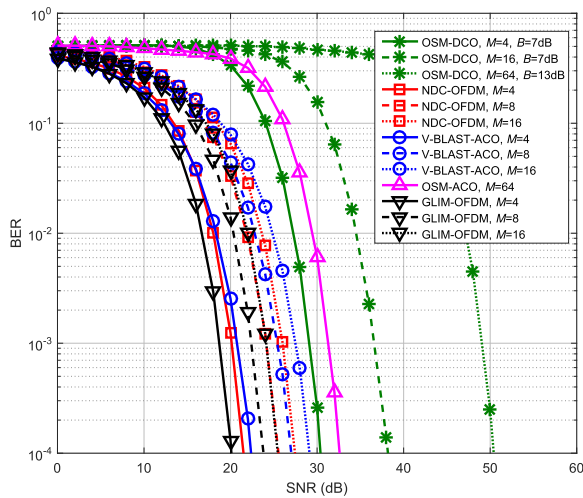

Fig. 7. BER performance comparison of optical MIMO-OFDM schemes for 2 (straight), 3 (dashed) and 4 (dotted) bits/s/Hz in physical channel $\mathbf{H}_B^p$.

Fig. 9. BER performance comparison of optical MIMO-OFDM schemes for 2 (straight), 3 (dashed) and 4 (dotted) bits/s/Hz in physical channel $\mathbf{H}_C^p$.

Based on this explanation, we can firmly state that the curves presented in Fig. 4, obtained for $\mathbf{H}_A^a$, indicate that much better performance can be obtained for GLIM-OFDM than the other systems, while they yield similar performances for $\mathbf{H}_A^p$ as shown in Fig. 5. According to Table IV, the channel coefficients of $\mathbf{H}_A^a$ and $\mathbf{H}_A^p$ are very similar to each other and far from having a diagonal structure. Consequently, their BER performances are affected dominantly by the detection errors of the indices. On the other hand, the other reference systems in the presence of these channels are also under similar effects depending on their system structures. As a result, our extensive simulation studies have shown that such performance differences occur between GLIM-OFDM and the other schemes as indicated in Figs. 4 and 5.

In Figs. 6 and 7, we compare the proposed system with other reference MIMO systems in the presence of the analytical and physical channel configurations $\mathbf{H}_B^a$ and $\mathbf{H}_B^p$, which have a modest diagonal structure with $d_{Tx} = 0.8$ m (Config B). The
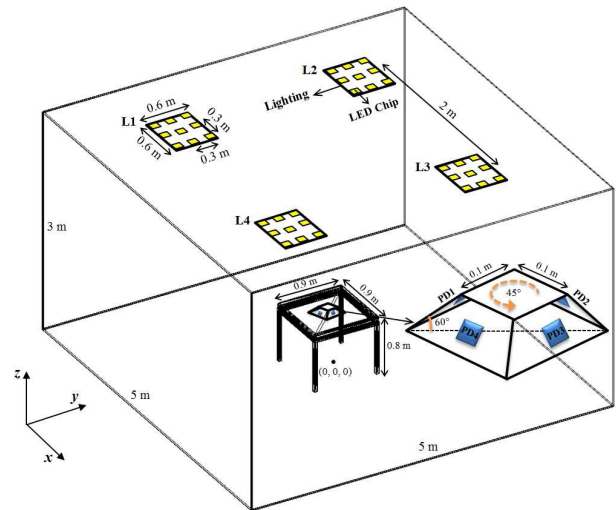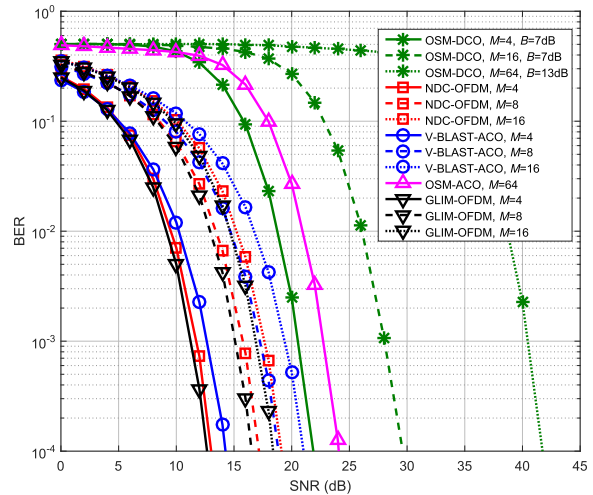
results presented in these figures show that the GLIM-OFDM scheme provides better BER performance than any other system with the same spectral efficiency. Since the proposed MAP estimator of GLIM-OFDM takes a-priori information into account, it always produces non-negative estimates based on the assumption that the signal has a unipolar p.d.f.

We now consider a modified implementation scenario for Config A ($d_{Tx} = 0.1$ m) to make it more suitable for the MAP estimator by introducing a slight tilt on the PDs. In realistic VLC application scenarios, due to the random orientations of mobile terminals, PD's are considered to be located in various positions and tilts (receivers around laptop screen or on the aircraft seats etc.), resulting in the average channel matrix close to diagonal. Hence, on average, the performance of the proposed GLIM-OFDM is improved substantially when compared to the other schemes.

In Fig. 8, a specially designed VLC structure is shown, to increase the power of the LOS links. In this design,
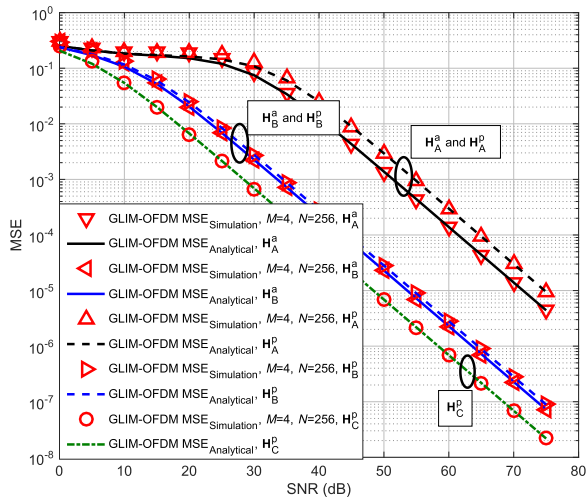
Fig. 10. Analytical and simulated MSE comparison for analytic channels, $\mathbf{H}_A^a$, $\mathbf{H}_B^a$ and physical channels $\mathbf{H}_A^p$, $\mathbf{H}_B^p$, $\mathbf{H}_C^p$.
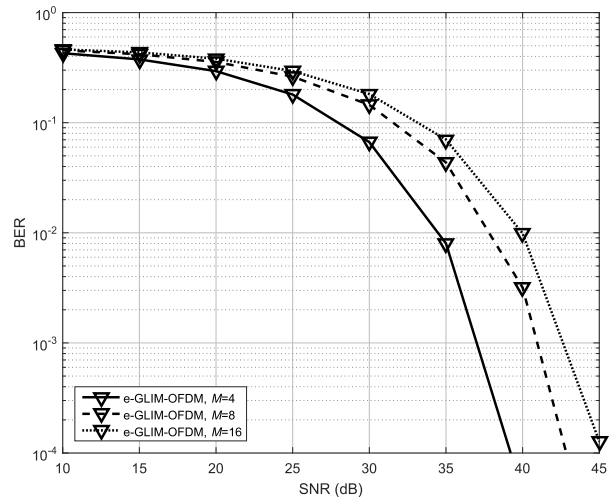

Fig. 11. BER performance of the enhanced-GLIM-OFDM (e-GLIM-OFDM) in frequency-selective MIMO VLC channels for 2 (straight), 3 (dashed) and 4 (dotted) bits/s/Hz.

the PDs are rotated 45° in the xy-plane and tilted 60° in the yz-plane. As a result, the Config C provides an increase in LOS link strength and hence, an increase in the correlation coefficient r of the channel matrix to make it more diagonal. The corresponding channel matrix, which is obtained by the physical model, can be given as

$$\mathbf{H}_C^p \approx 10^{-5} \times \begin{pmatrix} 0.5555 & 0.1866 & 0.1222 & 0.1866 \\ 0.1866 & 0.5555 & 0.1866 & 0.1222 \\ 0.1222 & 0.1866 & 0.5555 & 0.1866 \\ 0.1866 & 0.1222 & 0.1866 & 0.5555 \end{pmatrix}.$$

In Fig. 9, GLIM-OFDM is compared with other MIMO reference systems for 2, 3 and 4 bits/sec/Hz spectral efficiencies for the physical channel model of Config C with $d_{Tx} = 0.1$ m. The simulation results presented in Fig. 9 indicate that the proposed system uniformly outperforms of all other systems. Finally, in Fig. 10, the MSE vs. SNR curves are shown for GLIM-OFDM by employing both analytical and physical channel matrices. Moreover, theoretical MSE values are compared with the computer simulation results. We conclude from Fig. 10 that the theoretical and computer simulation curves match considerably well especially at high SNR values.

C. Performance of e-GLIM-OFDM

In this subsection, we present BER performance results of the e-GLIM-OFDM scheme. In Fig. 11, BER versus SNR curves are given for the e-GLIM-OFDM system operating at 2, 3 and 4 bits/sec/Hz spectral efficiency values in the presence of frequency-selective MIMO channels with six taps, which was described in Section IV-B. As seen from Fig. 11, the enhanced scheme also achieves similar BER performance compared to the first proposed scheme, which was operating over flat VLC channels. Since the proposed method takes the advantage of time and frequency domain transitions (by employing FFT/IFFT pair twice) and ZF equalizations, it can easily cope with both the inter-LED-interference (ILI) and ISI.

According to the computer simulation results, we can conclude that e-GLIM-OFDM is a feasible solution for the multi-path VLC channels. Since there do not exist any other frequency-selective MIMO-VLC based system in the literature, comparison with a reference system is not possible for the frequency-selective scenarios.

VI. CONCLUSIONS

VLC technologies, as well as the index modulation concept for MIMO systems, such as SM and subcarrier index modulation for OFDM are gaining noticeable attention for the next generation of wireless standards. In this paper, we have proposed two novel and spectral efficient 4×4 LED index modulation based optical MIMO-OFDM systems with MAP estimation, where the first scheme is operating in frequency-flat channels and the second one in frequency-selective channels. The proposed schemes offer twice the spectral efficiency as that of DCO-OFDM by exploiting the advantage of LED index modulation to avoid Hermitian symmetry and DC bias.

For the error performance analysis, five different physical channel models have been obtained. It has been concluded that the first proposed system yields the best BER performance in the lowest correlated and almost diagonal case of the channel matrix. In this particular model, the channel has been diagonalized by directed LEDs to PDs to obtain the most powerful LOS links. Among the other two physical and analytical models, the system has superior performance in the presence of analytical channel gains (i.e., LOS channel). This is mainly due to the fact that highly correlated physical channel gains degrade the performance of the MAP estimator to the level where it performs almost the same as the 4×4 NDC-OFDM system. Finally, we conclude from the computer simulations that the BER performance of the second designed VLC system does not significantly affected by the degree of frequency selectivity of the channel, while retaining its spectral efficiency advantage over other MIMO-OFDM based VLC systems.

Appendix
Frequency Selective CIRs

$\mathbf{g}_{1,1} \approx 10^{-8}[2.5107\ 1.3290\ 4.2021\ 5.2421\ 0.9347\ 0.4133]^T,$

$\mathbf{g}_{1,2} \approx 10^{-8}[13.869\ 4.3617\ 2.3950\ 0.4165\ 0.5569\ 0.2852]^T$

$\mathbf{g}_{1,3} \approx 10^{-8}[0.2502\ 2.5546\ 1.1561\ 1.0689\ 0.6099\ 0.5570]^T,$

$\mathbf{g}_{1,4} \approx 10^{-8}[16.220\ 4.4067\ 3.2170\ 1.6950\ 0.7968\ 0.2426]^T$

$\mathbf{g}_{2,1} \approx 10^{-8}[3.8362\ 1.2489\ 1.9733\ 2.8366\ 1.0588\ 0.7232]^T,$

$\mathbf{g}_{2,2} \approx 10^{-8}[257.69\ 9.0081\ 1.7300\ 2.9421\ 2.1824\ 0.2493]^T$

$\mathbf{g}_{2,3} \approx 10^{-8}[0.1758\ 3.5579\ 5.0503\ 1.2249\ 0.6706\ 0.2167]^T,$

$\mathbf{g}_{2,4} \approx 10^{-8}[127.47\ 10.155\ 0.1015\ 3.5622\ 2.7293\ 0.7926]^T$

$\mathbf{g}_{3,1} \approx 10^{-8}[130.23\ 8.0788\ 3.1797\ 1.7479\ 1.7082\ 0.3576]^T,$

$\mathbf{g}_{3,2} \approx 10^{-8}[0.1044\ 0.1007\ 0.6197\ 1.5607\ 0.5474\ 0.2261]^T$

$\mathbf{g}_{3,3} \approx 10^{-8}[0.4087\ 0.1467\ 3.0861\ 2.5029\ 0.3504\ 0.5618]^T,$

$\mathbf{g}_{3,4} \approx 10^{-8}[0.4368\ 2.9358\ 2.1694\ 2.1221\ 0.5044\ 0.4179]^T$

$\mathbf{g}_{4,1} \approx 10^{-8}[0.3185\ 6.2577\ 3.0124\ 0.9103\ 0.9437\ 0.4686]^T,$

$\mathbf{g}_{4,2} \approx 10^{-8}[5.1500\ 1.0373\ 1.9243\ 0.5546\ 0.1538\ 0.0613]^T$

$\mathbf{g}_{4,3} \approx 10^{-8}[0.4588\ 1.9667\ 3.4924\ 1.6399\ 0.6069\ 0.1007]^T,$

$\mathbf{g}_{4,4} \approx 10^{-8}[0.3313\ 13.331\ 2.8363\ 5.8317\ 1.4873\ 0.3917]^T$

Acknowledgment

References

[1] F. Miramirkhani and M. Uysal, "Channel modeling and characterization for visible light communications," *IEEE Photon. J.*, vol. 7, no. 6, Dec. 2015.

[2] Y. Tanaka, T. Komine, S. Haruyama, and M. Nakagawa, "Indoor visible communication utilizing plural white LEDs as lighting," in *Proc. 12th IEEE Int. Symp. Pers., Indoor Mobile Radio Commun. (PIMRC)*, vol. 2. Sep. 2001, pp. F-81–F-85.

[3] J. Armstrong and A. J. Lowery, "Power efficient optical OFDM," *Electron. Lett.*, vol. 42, no. 6, pp. 370–372, Mar. 2006.

[4] N. Fernando, Y. Hong, and E. Viterbo, "Flip-OFDM for optical wireless communications," in *Proc. IEEE Inf. Theory Workshop*, Paraty, Brazil, Oct. 2011, pp. 5–9.

[5] D. Tsonev and H. Haas, "Avoiding spectral efficiency loss in unipolar OFDM for optical wireless communication," in *Proc. IEEE Int. Conf. Commun. (ICC)*, Sydney, NSW, Australia, Jun. 2014, pp. 3336–3341.

[6] M. S. Islim, D. Tsonev, and H. Haas, "On the superposition modulation for OFDM-based optical wireless communication," in *Proc. IEEE Global Conf. Signal Inf. Process. (GlobalSIP)*, Orlando, FL, USA, Dec. 2015, pp. 1022–1026.

[7] Q. Wang, Z. Wang, and L. Dai, "Multiuser MIMO-OFDM for visible light communications," *IEEE Photon. J.*, vol. 7, no. 6, pp. 1–11, Dec. 2015.

[8] E. Basar, "Index modulation techniques for 5G wireless networks," *IEEE Commun. Mag.*, vol. 54, no. 7, pp. 168–175, Jul. 2016.

[9] R. Mesleh, H. Elgala, and H. Haas, "Optical spatial modulation," *IEEE/OSA J. Opt. Commun. Netw.*, vol. 3, no. 3, pp. 234–244, Mar. 2011.

[10] C. He, T. Q. Wang, and J. Armstrong, "Performance comparison between spatial multiplexing and spatial modulation in indoor MIMO visible light communication systems," in *Proc. IEEE Int. Conf. Commun. (ICC)*, Kuala Lumpur, Malaysia, May 2016, pp. 1–6.

[11] Y. Li, D. Tsonev, and H. Haas, "Non-DC-biased OFDM with optical spatial modulation," in *Proc. IEEE 24th Ann. Int. Symp. Pers., Indoor, Mobile Radio Commun. (PIMRC)*, London, U.K., Sep. 2013, pp. 486–490.

[12] K. Abe, C.-J. Ahn, T. Omori, and K.-Y. Hashimoto, "Spatial performance of color clustered VLC-MIMO due to incompleteness of color filters," in *Proc. Int. Symp. Intell. Signal Process. Commun. Syst. (ISPACS)*, Nusa Dua, Indonesia, Nov. 2015, pp. 417–421.

[13] Y. Chen and M. Jiang, "Joint colour-and-spatial modulation aided visible light communication system," in *Proc. IEEE 83rd Veh. Technol. Conf. (VTC Spring)*, Nanjing, China, May 2016, pp. 1–5.

[14] W. Xu, J. Wang, H. Shen, and H. Zhang, "Multi-colour LED specified bipolar colour shift keying scheme for visible light communications," *Electron. Lett.*, vol. 52, no. 2, pp. 133–135, Jan. 2016.

[15] P. Luo *et al.*, "Experimental demonstration of RGB LED-based optical camera communications," *IEEE Photon. J.*, vol. 7, no. 5, pp. 1–12, Oct. 2015.

[16] A. H. Azhar, T. A. Tran, and D. O'Brien, "A gigabit/s indoor wireless transmission using MIMO-OFDM visible-light communications," *IEEE Photon. Technol. Lett.*, vol. 25, no. 2, pp. 171–174, Jan. 15, 2013.

[17] A. Nuwanpriya, A. Grant, S.-W. Ho, and L. Luo, "Position modulating OFDM for optical wireless communications," in *Proc. IEEE Globecom Workshops*, Anaheim, CA, USA, Dec. 2012, pp. 1219–1223.

[18] T. Fath and H. Haas, "Optical spatial modulation using colour LEDs," in *Proc. IEEE Int. Conf. Commun. (ICC)*, Budapest, Hungary, Jun. 2013, pp. 3938–3942.

[19] T. Fath, J. Klaue, and H. Haas, "Coded spatial modulation applied to optical wireless communications in indoor environments," in *Proc. IEEE Wireless Commun. Netw. Conf. (WCNC)*, Apr. 2012, pp. 1000–1004.

[20] S. Dimitrov and H. Haas, *Principles of LED Light Communications: Towards Networked Li-Fi*. Cambridge, U.K.: Cambridge Univ. Press, 2015.

[21] S. M. Kay, *Fundamentals Statistical Signal Processing: Estimation Theory*. Upper Saddle River, NJ, USA: Prentice-Hall, 1993.

[22] T. Komine and M. Nakagawa, "A study of shadowing on indoor visible-light wireless communication utilizing plural white LED lightings," in *Proc. 1st Int. Symp. Wireless Commun. Syst.*, Port-Louis, Mauritius, Sep. 2004, pp. 36–40.

[23] P. Chvojka, S. Zvanovec, P. A. Haigh, and Z. Ghassemlooy, "Channel characteristics of visible light communications within dynamic indoor environment," *IEEE J. Lightw. Technol.*, vol. 33, no. 9, pp. 1719–1725, May 1, 2015.

[24] A. T. Hussein and J. M. H. Elmirghani, "Performance evaluation of multi-gigabit indoor visible light communication system," in *Proc. 20th Eur. Conf. Netw. Opt. Commun. (NOC)*, London, U.K., Jun. 2015, pp. 1–6.

[25] K. Lee, H. Park, and J. R. Barry, "Indoor channel characteristics for visible light communications," *IEEE Commun. Lett.*, vol. 15, no. 2, pp. 217–219, Feb. 2011.

[26] J. Ding, K. Wang, and Z. Xu, "Impact of LED array simplification on indoor visible light communication channel modeling," in *Proc. 9th Int. Symp. Commun. Syst., Netw. Digit. Signal Process. (CSNDSP)*, Manchester, U.K., Jul. 2014, pp. 1159–1164.

[27] *Lighting of Indoor Work Places*, document ISO 8995:2002 CIE S 008/E-2001, International Standard, 2015.

[28] F. Miramirkhani, M. Uysal, and E. Panayirci, *Channel Modeling for Visible Light Communications*. Cham, Switzerland: Springer, 2016, pp. 107–122.

[29] M. Uysal *et al.*, *TG7r1 Channel Model Document For High-Rate PD Communications*, document IEEE 802.15-15/0746r1, Sept. 2015.

[30] R. Mesleh, H. Elgala, and H. Haas, "Optical spatial modulation," *IEEE/OSA J. Opt. Commun. Netw.*, vol. 3, no. 3, pp. 234–244, Mar. 2011.

[31] S. D. Dissanayake and J. Armstrong, "Comparison of ACO-OFDM, DCO-OFDM and ADO-OFDM in IM/DD systems," *J. Lightw. Technol.*, vol. 31, no. 7, pp. 1063–1072, Apr. 1, 2013.

[32] T. Fath and H. Haas, "Performance comparison of MIMO techniques for optical wireless communications in indoor environments," *IEEE Trans. Commun.*, vol. 61, no. 2, pp. 733–742, Feb. 2013.

Anil Yesilkaya (S'11) received the B.Sc. (Hons.) and M.Sc. degrees in electronics engineering from Kadir Has University, Istanbul, Turkey, in 2014 and 2016, respectively. He is currently pursuing the Ph.D. degree with the Institute for Digital Communications, The University of Edinburgh. His current research interests include multiple-input multiple-output visible light communications and LiFi-based networking for aeronautical cabin applications.

Ertugrul Basar (S'09–M'13–SM'16) received the B.S. degree (Hons.) from Istanbul University, Turkey, in 2007, and the M.S. and Ph.D. degrees from Istanbul Technical University in 2009 and 2013, respectively. He spent the academic year 2011-2012 with the Department of Electrical Engineering, Princeton University, NJ, USA. He was an Assistant Professor with Istanbul Technical University from 2014 to 2017, where he is currently an Associate Professor of Electronics and Communication Engineering. His primary research interests include MIMO systems, index modulation, cooperative communications, OFDM, and visible light communications. He is an inventor of two pending patents on index modulation schemes. He was a recipient of the Istanbul Technical University Best Ph.D. Thesis Award in 2014 and has received three best paper awards including one from the IEEE International Conference on Communications 2016. He currently serves as an Associate Editor of IEEE COMMUNICATIONS LETTERS and the IEEE ACCESS. He is also a Regular Reviewer of various IEEE journals, and has served as a TPC member for several conferences.

Farshad Miramirkhani (M'13) received the B.Sc. and M.Sc. degrees (Hons.) in electronics and communication engineering from the University of Isfahan, Isfahan, Iran, in 2011 and 2014, respectively. He is currently pursuing the Ph.D. degree with the Communication Theory and Technologies (CT&T) Research Group under the supervision of Prof. M. Uysal with Ozyegin University, Istanbul, Turkey. He joined the CT&T Research Group as a Research Assistant in 2014. The LiFi channels developed by Prof. M. Uysal and Mr. Miramirkhani were selected as the LiFi Reference Channel Models by the IEEE 802.15.7r Task Group during the IEEE's latest meeting held in Bangkok, Thailand, in 2015. His current research interests include optical wireless communications, indoor visible light communications, underwater visible light communications and channel modeling. He has served as a reviewer for several prestigious journals and conferences for the IEEE and OSA societies.

Erdal Panayirci (M'80–SM'91–F'03–LF'06) received the Diploma Engineering degree in electrical engineering from Istanbul Technical University, Istanbul, Turkey, and the Ph.D. degree in electrical engineering and system science from Michigan State University, USA. Until 1998 he has been with the Faculty of Electrical Engineering, Istanbul Technical University, where he was a Professor and the Head of the Telecommunications Chair. He is currently a Professor of Electrical Engineering and the Head of the Electrical and Electronics Engineering Department with Kadir Has University, Istanbul. He has been the Principal Coordinator of a 6th and 7th Frame European Project called the Network of Excellent on Wireless Communications and WIMAGIC Strep Project for two years, representing Kadir Has University. He has authored extensively in leading scientific journals and international conference and co-authored the book *Principles of Integrated Maritime Surveillance Systems* (Boston, Kluwer Academic Publishers, 2000). His recent research interests include communication theory, advanced signal processing techniques and their applications to wireless electrical, underwater, and optical communications. He was an Editor of the IEEE TRANSACTIONS ON COMMUNICATIONS in the areas of synchronizations and equalizations from 1995 to 2000. He served as a member of IEEE Fellow Committee from 2005 to 2008. He was the Technical Program Co-Chair of the IEEE International Conference on Communications and the Technical Program Chair of the IEEE PIMRC held in Istanbul, in 2006 and 2010, respectively. He was the Executive Vice-Chairman of the upcoming IEEE Wireless Communications and Networking Conference held in Istanbul in 2014. He is currently a member of the IEEE GLOBECOM/ICC Management and Strategy Standing Committee and the Head of the Turkish Scientific Commission on Signals and Systems of International Union of Radio Science.

Murat Uysal (M'98–SM'07) received the B.Sc. and M.Sc. degree in electronics and communication engineering from Istanbul Technical University, Istanbul, Turkey, in 1995 and 1998, respectively, and the Ph.D. degree in electrical engineering from Texas A&M University, College Station, TX, USA, in 2001. He was a tenured Associate Professor with the University of Waterloo, Canada, where he currently holds an adjunct faculty position. He is currently a Full Professor and the Chair of the Department of Electrical and Electronics Engineering, Ozyegin University, Istanbul. He also serves as the Founding Director of the Center of Excellence in optical wireless communication technologies. His research interests are in the broad areas of communication theory and signal processing with a particular emphasis on the physical layer aspects of wireless communication systems in radio and optical frequency bands. He has authored some 270 journal and conference papers on these topics and received over 7000 citations. He currently serves on the Editorial Board of the IEEE TRANSACTIONS ON WIRELESS COMMUNICATIONS. He was an Editor of the IEEE TRANSACTIONS ON COMMUNICATIONS, the IEEE TRANSACTIONS ON VEHICULAR TECHNOLOGY, the IEEE COMMUNICATIONS LETTERS, the *Wiley Wireless Communications and Mobile Computing Journal*, the *Wiley Transactions on Emerging Telecommunications Technologies*, and a Guest Editor of the IEEE JSAC Special Issues on Optical Wireless Communication in 2009 and 2015. He was involved in the organization of several IEEE conferences at various levels. He served as the Chair of the Communication Theory Symposium of IEEE ICC 2007, the Chair of the Communications and Networking Symposium of the IEEE CCECE 2008, the Chair of the Communication and Information Theory Symposium of IWCMC 2011, the TPC Co-Chair of the IEEE WCNC 2014, and the General Chair of IEEE IWOW 2015. Over the years, he has served on the Technical Program Committee of over 100 international conferences and workshops in the communications area. His distinctions include the Marsland Faculty Fellowship in 2004, the NSERC Discovery Accelerator Supplement Award in 2008, the University of Waterloo Engineering Research Excellence Award in 2010, the Turkish Academy of Sciences Distinguished Young Scientist Award in 2011, and the Ozyegin University Best Researcher Award in 2014.

Harald Haas (S'98–AM'00–M'03–SM'17) received the Ph.D. degree from the University of Edinburgh, Edinburgh, U.K., in 2001. He is currently the Chair of Mobile Communications with The University of Edinburgh, and the Founder and Chief Scientific Officer of pureLiFi Ltd., Edinburgh, U.K., and the Director of the LiFi Research and Development Center, The University of Edinburgh. His main research interests include optical wireless communications, hybrid optical wireless and RF communications, spatial modulation, and interference coordination in wireless networks. He first introduced and coined spatial modulation and LiFi. LiFi was listed among the 50 best inventions in *TIME Magazine 2011*. He was an Invited Speaker at TED Global 2011, and his talk Wireless Data from Every Light Bulb has been watched online over 2.4 million times. He gave the second TED Global lecture in 2015 on the use of solar cells as LiFi data detectors and energy harvesters, which was viewed online over 17 million times. He holds 43 patents and has over 30 pending patent applications. He has authored 400 conference and journal papers including a paper in science. He co-authored a book *Principles of LED Light Communications Towards Networked Li-Fi* (Cambridge University Press, 2015). He was a co-recipient of Best Paper Award at the IEEE Vehicular Technology Conference in Las Vegas in 2013 and VTC in Glasgow in 2015. He was a co-recipient of the EURASIP Best Paper Award for the *Journal on Wireless Communications and Networking* in 2015, and a co-recipient of the Jack Neubauer Memorial Award of the IEEE Vehicular Technology Society. In 2012, he received the prestigious Established Career Fellowship from the Engineering and Physical Sciences Research Council within Information and Communications Technology in the U.K. He received the Tam Dalyell Prize 2013 from The University of Edinburgh for excellence in engaging the public with science. In 2014, he was selected by the EPSRC as one of ten Recognizing Inspirational Scientists and Engineers Leaders in the U.K. He was a recipient of the Outstanding Achievement Award of the International Solid State Lighting Alliance in 2016 and he was an elected fellow of the Royal Society of Edinburgh in 2017.